Progress In Electromagnetics Research C, Vol. 25, 1–14, 2012

PACKAGED CMOS TRANSMISSION LINE BASED ACTIVE BANDPASS FILTER WITH HIGH STOPBAND SUPPRESSION

M.-L. Lee[1,*], H.-S. Wu[2], and C.-K. C. Tzuang[1]

[1]Graduate Institute of Communication Engineering, National Taiwan University, No. 1, Sec. 4, Roosevelt road, Taipei 106, Taiwan

[2]School of Electronic Information Engineering, Tianjin University, Tianjin 300072, China

Abstract—This paper presents a packaged third-order transmission line based (TL-based) active bandpass filter (BPF), which is fabricated using Silterra's standard 0.18-µm CMOS 1P6M technology, with high stopband suppression. The active compensating circuit, which produces negative conductance, improves the quality factor (Q factor) of TL-based resonator and suppresses the spurious resonances at even-harmonic frequencies. The spurious responses are also shifted towards higher frequencies by applying a capacitively loaded TL resonator to the filter design. Additionally, an inductive parasitic effect introduced by the package is investigated and reduced to achieve the minimum impact on the stopband suppression. Measurement results indicate that the prototype has an insertion loss of 0.95 dB at a central frequency (f_0) of 1.53 GHz with a 3-dB bandwidth of 3.1%, while a current of 8 mA is consumed from 3.0 V. The stopband suppressions at $2f_0$ and $3f_0$ are 44.57 dB and 52.78 dB, respectively. Furthermore, the suppression exceeds 35 dB from $1.09f_0$ to $10.05f_0$.

1. INTRODUCTION

Rapid advances in wireless communication systems are driving the miniaturization and cost reduction of the radio frequency (RF) bandpass filters (BPFs). To fulfill these requirements, [1–4] are implemented with the technologies of planar printed circuit board (PCB) and low temperature co-fired ceramic (LTCC). Stopband suppression is required for BPF designs in the congested

Received 9 August 2011, Accepted 13 October 2011, Scheduled 19 October 2011

* Corresponding author: Meng-Lin Lee (d94942008@ntu.edu.tw).

spectrum below 6 GHz. The techniques, including the stepped-impedance resonator (SIR) [5] and stub-loaded multiple-mode resonator (MMR) [6], have been reported. Parallel to the filters on the laminated substrate, the monolithic filters, which integrate the active circuits to maintain the Q factor of resonators on a semiconductor substrate, demonstrate the superior characteristics on the frequency selectivity, gathering more attentions from the system integration [7–13]. These successful developments focus on reducing the passband loss [7, 9, 12], improving the linearity [8], and maintaining the passband flatness [10, 11, 13]. Few designs discuss the minimization of spurious responses of the active BPF. This paper presents a comprehensive design from the chip to the package to develop the active BPF with the wide stopband suppression. Section 2 reports the analyses of the resonator syntheses in details, showing the design approach for the spurious reduction. Section 3 shows the package design of the RF active BPF and examines the impact of the package parasitic on the stopband suppression. Section 4 presents the experimental results of the prototypes from the wafer to the package for validating the feasibility of the proposed design. The measurement results show the packaged filter has an insertion loss of 0.95 dB at 1.53 GHz in the 3.1% 3-dB bandwidth. The stopband suppression is higher than 35 dB from $1.09f_0$ to $10.05f_0$. Section 5 concludes this paper.

2. CMOS TL-BASED ACTIVE BPF WITH WIDE STOPBAND SUPPRESSION

Figure 1 shows the schematic of a transmission line (TL)-based active BPF in a order of three and the photograph of the prototype fabricated in Silterra's 0.18-μm CMOS 1P6M (one-poly six-metal) foundry. Two gate-grounded nMOS transistors (M_1 and M_2), which form the PS- and NS-mode current discharging paths, are inserted into the input and output ports for the electrostatic discharge (ESD) protection [14]. The capacitors (C_{01} and C_{12}), which form the immittance inverters, define the adjacent coupling between the composite resonators. These capacitances can be calculated by following the documented procedures with the specific bandwidth and the rejection [15].

The on-chip synthetic TL, which is loaded by the capacitors and the degenerated cross-coupled pair, implements the composite resonators in the monolithic filter [13]. The cross-coupled pair produces the negative conductance of $-g_m/2$ to compensate for the loss of the TL, increasing the quality factor (Q factor) of a resonator [9]. The practical comparisons based on the same foundry technology reveal the transmission line in Fig. 1(b) has the attractive advantages on the

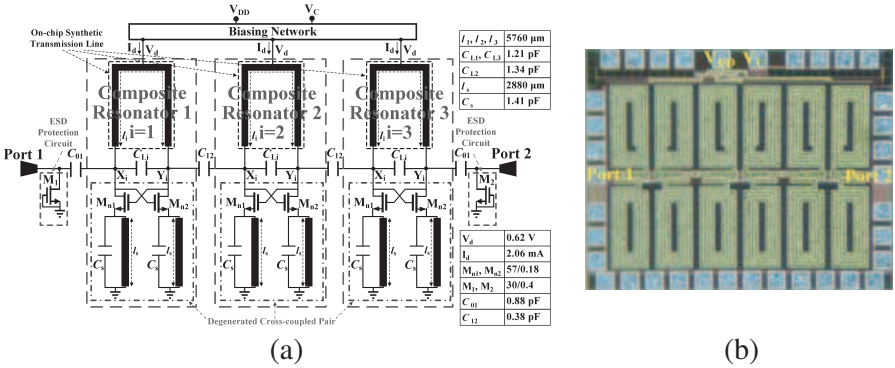

Figure 1. 1.55 GHz third-order CMOS TL-based active BPF. (a) Schematic. (b) Prototype in Silterra's 0.18-µm CMOS 1P6M foundry with a chip area of 1.24 mm by 0.92 mm and a wafer thickness of 480 µm.

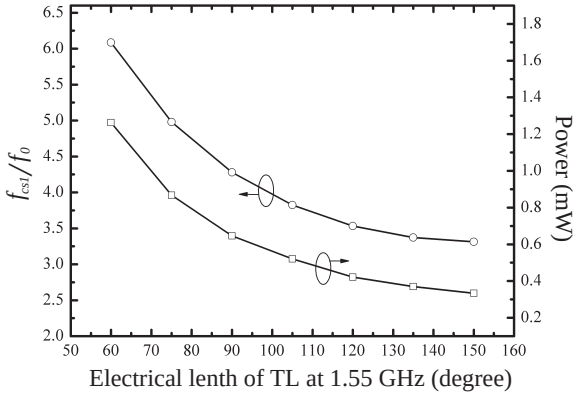

Figure 2. The power consumptions and spurious responses of the composite resonators at 1.55 GHz.

syntheses of the high characteristic impedance (Z_c) and the circuit miniaturization [13]. The behaviors of the composite resonator had been carefully analyzed based on its equivalent circuit. The design equations, which are theoretically and experimentally validated, can be applied to synthesize the conductance of a resonator as a constant value, which approaches zero, in a certain bandwidth, improving the passband flatness [13]. The analyses disclosed in [13] only focus on the filter inside the passband. The behavior of the composite resonator out of the passband and its impact on the spurious responses become the main object of this paper.

The cross-coupled pair can produce the negative conductance once the signals between two drain terminals are out of phase. As shown in Fig. 1(a), the TL and loaded capacitor (C_{Li}) form the parallel resonator to make the phase difference between the X_i and Y_i terminals, denoted by θ_{XY}, equal to 180° at the resonant frequency, establishing the Q enhancement of the resonator. However, due to the dispersive propagation of the physical TL, θ_{XY} can be equal to 180° above the passband, causing the spurious responses of the filter to be enhanced out of the passband. The filter phenomena mentioned above can be quantitatively investigated through the resonator designs. Fig. 2 shows the comparisons between the five composite resonators with the different length of TL. During the designs, the guiding properties and the characteristic impedance of the TL are identical to those of in [13]. All the resonators are designed with the identical cross-coupled pair to achieve the same Q factor at f_0 of 1.55 GHz. The commercial software, Aiglent ADS 2009, is applied to perform the circuit simulations for observing the input impedance magnitude of the resonators. Since composite resonator in Fig. 1(a) forms the parallel resonance, the input impedance magnitude has a first peak at f_0, and the other peaks above due to the spurious phenomena. The f_{es1} in the Fig. 2 indicates the frequency of the second peak, implying the lowest frequency, at which the first spurious response occurs. The curve with hollow dots shows that the ratio of f_{es1} to f_0 increases from 3.31 to 6.09 when the electric length of the TL decreases from 150.6° to 60°, indicating the shift of the spurious responses away from the passband of the filter. The composite resonator constructed by the shorter TL can assist the filter in realizing wider stopband suppression. Additionally, the curve with hollow squares shows the power consumption of a resonator increases from 0.33 mW to 1.26 mW when the length of the TL decreases from 150.6° to 60°. Since the equivalent parallel resistance of the composite resonator is proportional to the length of the TL, the decreasing of the electric length reduces the Q factor of a resonator. Thus, the higher negative conductance from the cross-coupled pair is required for Q enhancement. The comparisons summarized above show the design approach for the monolithic active BPF to minimize the spurious responses. Additionally, the curves in Fig. 2 reveal the trade-off design between the spurious suppression and the power consumption of the proposed active BPF.

3. PACKAGED OF CMOS ACTIVE BPF

The package for the proposed active BPF is realized by using the standard chip-on-board (COB) process. Fig. 3 shows the concept

of the package implementation. The board is made of a two-layer laminated substrate, RO4003, with a thickness of 0.508 mm and a relative permittivity of 3.38. The fabricated chip shown in Fig. 1(b) is attached to the board with the silver glue. The connections between the chip and board are built by the wire bonding. Owing to the lack of ground via holes in the standard CMOS technology, the parasitic, introduced by the bondwires, substantially affects the frequency response, and needs to be characterized. Fig. 4 shows the equivalent circuit of the proposed filter, including the package effect. L_{RF} and L_{gnd} represent the inductances of the bondwires at two RF ports and the ground of the monolithic filter. L_{gnd} and the capacitive characteristic of the composite resonator cause the series resonance, generating the additional transmission zero above the passband to disturb the stopband suppression [16]. To investigate the impacts of the L_{RF} and L_{gnd} on the proposed BPF, the commercial software, ANSYS HFSS, is applied to extract the equivalent inductances of the

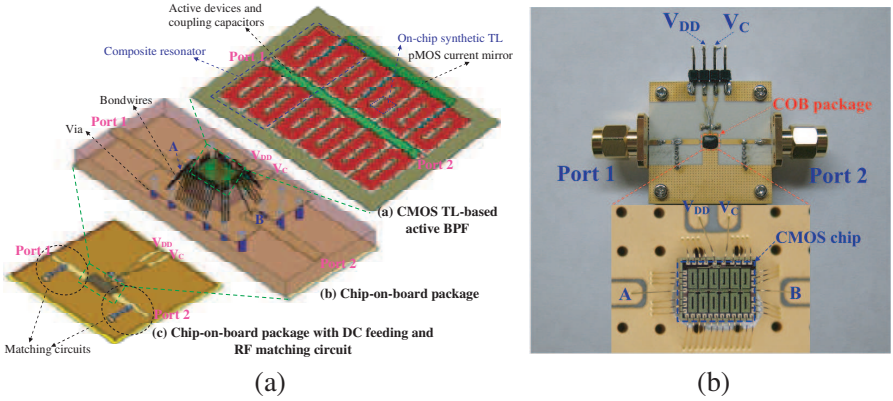

(a) (b)

Figure 3. (a) Architecture of the COB package and the test module. (b) Complete COB package and the test module.

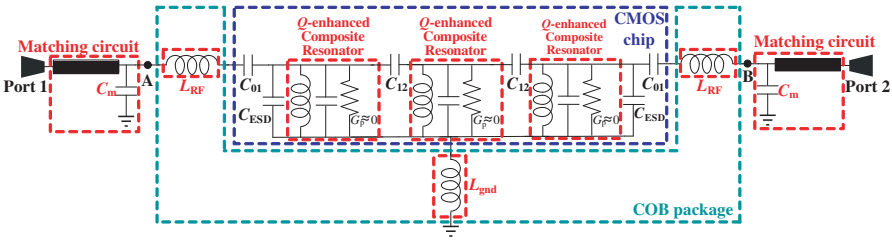

Figure 4. Equivalent circuit of the packaged filter in Fig. 3(b).

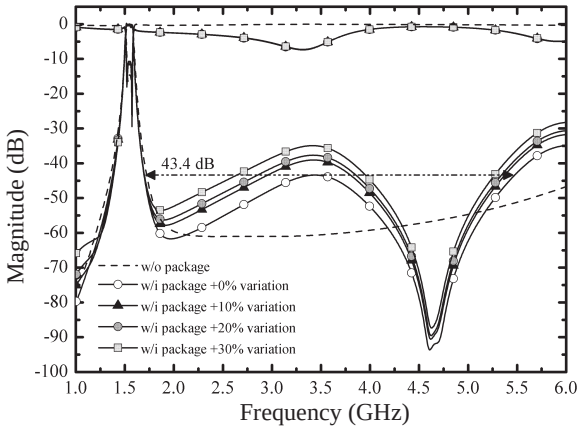

Figure 5. The simulated frequency responses of the CMOS active BPF.

bondwires. In the HFSS simulations, all bondwires are made of gold with a diameter of 25.4 μm. The chip and bondwires are covered entirely by the plastic encapsulant with a relative permittivity of 9.2. As shown in Figs. 3(a) and 3(b), L_{RF}, which is generated by a bondwire with a length of 1.3 mm, is 1.5 nH and degrades the in-band return loss. Thus, the external matching circuit is designed to absorb the L_{RF}. A ground bondwire has a length of 1.14 mm and generates an inductance of 1.1 nH. As the number of ground bondwires increases to 32, L_{gnd} is produced as 0.072 nH. The extracted inductances are imported into the circuit simulations, conducted by using the software, Agilent ADS 2009, for evaluating the package effects on the frequency response. Fig. 5 shows the ADS simulation results of the filter design, including the bondwire inductances, showing the central frequency of 1.546 GHz with an insertion loss of 0 dB. The filter design presented in this paper is identical to those of in [13] except the passband bandwidth and the additional ESD protection. The bandwidth is 3.1% at 1.55 GHz, 61.3% narrower than in [13].

The curves with hollow dots indicate that the ground bondwires cause a transmission zero at 4.61 GHz and disturb the flatness of the frequency response above 2 GHz, compared with the dashed curve, which represents the CMOS TL-based active BPF without a package. Additionally, the stopband suppressions at $2f_0$ and $3f_0$ are 46.2 dB and 92.6 dB, respectively. Upper stopband suppression of the prototype in Fig. 3(b) from 1.7 GHz to 5.48 GHz reduces to 43.4 dB, compared with the CMOS TL-based active BPF without a package. However, the variation in the length of the bondwires is unavoidable in the

package fabrication. As the length per bondwire varies from +10% to +30%, L_{gnd}, which is estimated by HFSS simulations, increases from 0.096 nH to 0.124 nH. The curves in Fig. 5 shows the two-port simulated S-parameters with variations in length per bondwire from +10% to +30%. When the variation increases from from 0% to +30%, the suppressions at $2f_0$ and $3f_0$ are degraded from 46.2 dB to 37.2 dB and 92.6 dB to 87.2 dB, respectively. The suppression from 1.7 GHz to 5.48 GHz is decreased from 43.4 dB to 34.9 dB. The curves in Fig. 5 show the impact of the variation in bondwires on the stopband suppression, revealing the acceptable tolerance in the package processes.

4. MEASUREMENTS

On-wafer two-port measured S-parameters of the CMOS TL-based active BPF in the 50-Ω system are obtained using an Agilent E8361C PNA (Performance Network Analyzer) and Picoprobe® un-balanced SG and GS probes. The output power of the PNA is set to −25.0 dBm in the small-signal experiments and short-open-load-through (SOLT) calibration procedures are carried out. The contact pads applied to the RF input/output ports are deembeded. The insertion loss is as high as 37 dB with zero power consumption (V_{C} and V_{DD} are set to 0 V) in Fig. 6(a). A composite resonator consumes 1.28 mW (2.06 mA) from a V_d of 0.62 V. The prototype in Fig. 1(b), including the complete biasing network, consumes 21 mW (7 mA) from a V_{DD} of 3.0 V while V_{C} is set to 2 V. On-wafer measurement results, represented

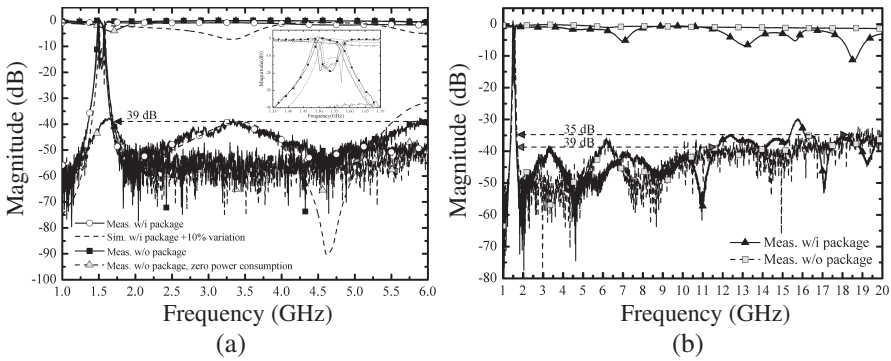

Figure 6. Measured two-port S-parameters of the CMOS TL-based active BPF with/without package in 50-Ω system. (a) From 1 to 6.0 GHz. (b) From 1 GHz to 20 GHz.

by the curve with squares in Fig. 6(a), show 0.98 dB insertion loss at 1.536 GHz and 47.4 MHz (3.1%) 3-dB bandwith with 15 dB return loss within the passband. The composite resonator is designed based on a major assumption that the two nMOS transistors are identical. The process variation, which produces the transistor mismatch, affects the precision of the compensation for the passband flatness. Moreover, the variation, which makes the change of the parasitic capacitances of the nMOS cross-coupled pairs, produces the drift of the central frequency from 1.55 GHz to 1.536 GHz. The wide-band measurement results, represented by the curves with squares in Fig. 6(b), demonstrate the wide upper stopband, extended from $1.1f_0$ to $11.8f_0$ (f_0 is 1.536 GHz), for the suppression level of 35 dB and confirm the design approach for wider stopband suppression in Section 2.

The two-port S-parameters of the prototype in Fig. 3(b) are measured with Agilent E8364B PNA after short-open-load-through (SOLT) calibration procedures are conducted in the 50-Ω system. The output power of the PNA is set to -25 dBm. The prototype in Fig. 3(b) consumes 24 mW (8.0 mA) from a V_{DD} of 3.0 V at a V_{C} of 2.2 V. Additional 3-mW power (1-mA current) is consumed to compensate for the loss, which is generated from RF bondwires and matching circuits. According to the curves hollow dots in Fig. 6(a), measurement results agree with the simulation ones with the $+10\%$ variation in length per bondwire. The central frequency, f_0, is 1.53 GHz with a 0.95 dB insertion loss, and the 3-dB bandwidth is 47.4 MHz (3.1%) with a return loss of 15 dB. The quality factor of a bandpass filter is defined as the ratio of the central frequency to the 3-dB bandwith [17]. Thus, the quality factor of the prototype in Fig. 3(b) is 32.3. However, in Fig. 6(a), because of the CMOS process variation, the central frequency shifts down from 1.546 GHz to 1.53 GHz. In Fig. 6(a), a transmission zero appears at 4.64 GHz; in addition, the measured stopband suppressions at $2f_0$ and $3f_0$ are 44.57 dB and 52.78 dB, respectively. In Fig. 6(b), the curves with triangles, represents the prototype in Fig. 3(b), shows that upper stopband suppression from $1.08f_0$ to $7.66f_0$ is maintained at higher than 39 dB. Otherwise, the wide upper stopband is extended from $1.09f_0$ to $10.05f_0$, for the suppression level of 35 dB in Fig. 6(b).

The noise figure (NF) and nonlinear characteristics are measured as follows. At a room temperature of 27°C in the 50-Ω system, the measured NF within the entire passband is maintained below 17.6 dB in Fig. 7(a). The relationship between the NF of the active devices and the filter are analyzed and reported in the section IV of [9]. By properly selecting the size and the biasing point of the nMOS cross-coupled pair, the noise of the active device can be reduced, resulting

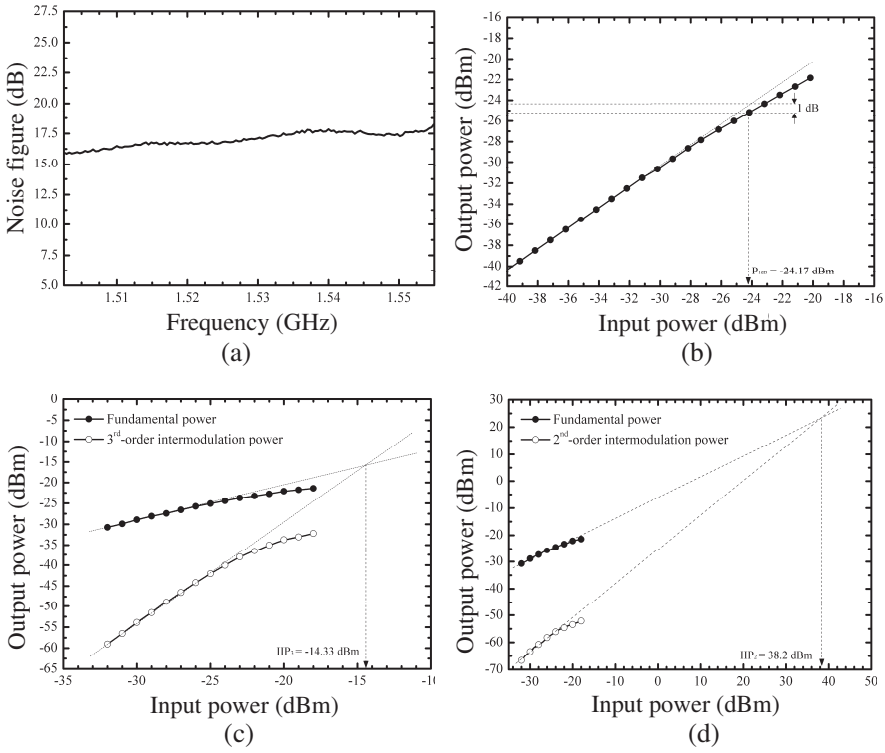

Figure 7. (a) Measured NF. (b) Measured 1-dB compression point ($P_{1\mathrm{dB}}$). (c) Measured input 3rd-order intermodulation intercept point (IIP_3). (d) Measured input 2nd-order intermodulation intercept point (IIP_2) of the prototype in Fig. 3(b).

in the NF improvement of the prototype. The measured input 1-dB compression point ($P_{1\mathrm{dB}}$) is $-24.17\,\mathrm{dBm}$ at 1.53 GHz in Fig. 7(b). To measure the effect of the intermodulation, the two test signals, which are set at 1.525 and 1.535 GHz, are sent to the prototype in Fig. 3(b), resulting in the in-band third-order intermodulation products at 1.515 and 1.545 GHz and the second-order intermodulation product at 3.06 GHz, respectively. The measured input third-order intermodulation intercept point (IIP_3) is $-14.33\,\mathrm{dBm}$ in Fig. 7(c). Otherwise, the high stopband suppression at $2f_0$, as shown in Fig. 6(a), causes the measured input second-order intermodulation intercept point (IIP_2) to reach 38.2 dBm in Fig. 7(d). In the schematic of Fig. 1(a), the unbalanced loads at the two drain terminals, X_i and Y_i, of an nMOS cross-coupled pair initially limit the linearity of the

prototype. For the requested frequency response, the linearity of the prototype can be improved by properly selecting the susceptance slope parameter, which is related to the guiding characteristics of the on-chip synthetic TL, of the composite resonator to reduce the difference in coupling capacitance between C_{01} and C_{12}. The capability of Human-Body Model (HBM) ESD protection at RF port under PS and NS modes is tested. The RF port is stressed from 0.25 kV (-0.25 kV) with 0.25 kV increase (decrease) per step, and the prototype in Fig. 3(b) can sustain 0.5 kV in PS mode and -1 kV in NS mode at RF ports.

To evaluate the temperature variable, the prototype in Fig. 3(b) is placed in a programmable temperature chamber, which varies the

Table 1. Summary of V_{C}, consumed currents and central frequencies from -40°C to +80°C.

Temperature (°C)	V_C (V)	Consumed current (mA)	Central frequency (GHz)
+80	3.78	13	1.479
+60	3.05	11	1.496
+40	2.52	9	1.516
+20	2.12	8	1.534
0	1.77	6	1.551
−20	1.54	5	1.568
−40	1.31	4	1.587

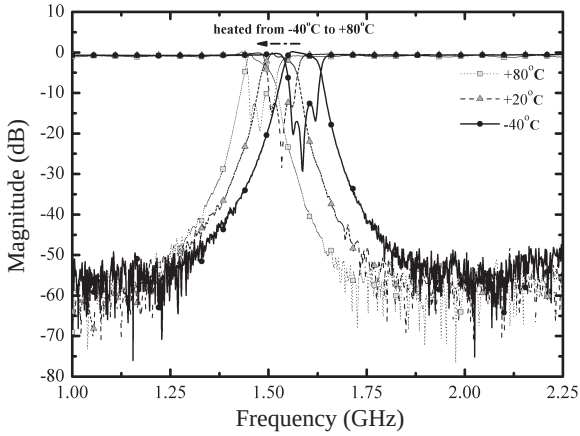

Figure 8. Measured S-parameters of the prototype in Fig. 3(b) with the temperature varied ranging from -40°C to +80°C.

temperature from −40°C to +80°C and increases by +20°C. For the temperature characteristic of the semiconductor, under the fixed size, bias voltage and the consumed current, the transistor provides a higher g_m at a low temperature and provides a lower g_m at a high temperature. Therefore, to maintain the insertion loss at a central frequency lower than 1 dB at different temperatures, a larger consumed current is required at a high temperature by increasing V_C; in addition, a lower consumed current is required at a low temperature by decreasing V_C. Table 1 summarizes the consumed currents, values of V_C, and central frequencies for the prototype in Fig. 3(b) at different temperatures under constant V_{DD} of 3.0 V. According to this table, during heating from −40°C to +80°C, the consumed current increases from 4 mA to 13 mA and V_C increases from 1.31 V to 3.78 V. Fig. 8 illustrates the measured S-parameters for the temperature variation, and the central frequency shifts from 1.587 to 1.479 GHz with a shift rate of −0.9 MHz/°C from −40°C to +80°C. The central frequency shift results mainly from the parasitic capacitor, which proportionally varies with the bias voltage of a transistor. Thus, the central frequency shifts down with an increasing V_C.

Table 2 summarizes the RF monolithic active BPFs, but the stopband suppression is rarely discussed in the present literature. In

Table 2. Comparison of RF monolithic active bandpass filter.

Prototype	[7]	[8]	[9]	[10]	[11]	[12]	This work
Process	CMOS 0.18 μm	CMOS 0.18 μm	CMOS 0.18 μm	CMOS 0.25 μm	CMOS 0.18 μm	GaAs 1 μm MESFET	CMOS 0.18 μm
Chip area (mm^2)	0.63	2.25	1.08	1.89	0.81	4.96	0.86 #
f_0 (GHz)	2.5	2.36	6.02	2.14	2.03	2.27	1.53
A_N (%)	4.4×10^{-3}	1.4×10^{-2}	4.3×10^{-2}	9.6×10^{-3}	3.7×10^{-3}	2.8×10^{-2}	2.2×10^{-3}
Order	2	3	2	3	4	3	3
BW (%)	28	2.54	18.9	2.8	6.4	5	3.1
P_D (mW)	5.6 (7mA @0.8V)	8.8 (5.84mA @1.5V)	5.4 (3mA @1.8V)	5 (2mA @2.5V)	16.6 (9.2mA @1.8V)	300*	24* (8mA @3V)
Type-based	Lump	Lump	TL	Lump	Lump	Lump	TL
Package	w/o	w/o	w/o	w/o	w/o	w/i	w/i
SS (dB) @ $2f_0/3f_0$	-	-	22/24	-	-	>40*	44.6/52.8*
SS level /range	-	-	20 dB/ $1.36f_0$-$2.18f_0$	-	-	40 dB*/ $1.15f_0$-$4.19f_0$	39 dB*/ $1.08f_0$-$7.66f_0$ 35 dB*/ $1.09f_0$-$10.1f_0$

*Packaged measurement result #Not including bond pads

Table 2, SS means the stopband suppression and A_N is the chip area, which is normalized to the square of the free-space wavelength at the central frequency. This work, which is designed based on the TL, demonstrates the highest stopband suppression at $2f_0$ and $3f_0$, even with the package. Although the prototype in [12] shows the stopband suppression better than 40 dB up to $4.19f_0$, this work can achieve wider stopband from $1.08f_0$ to $7.66f_0$ for the suppression level of 39 dB and from $1.09f_0$ to $10.05f_0$ for the suppression level of 35 dB.

5. CONCLUSION

This paper presents a packaged third-order 1.53 GHz CMOS TL-based active BPF with high stopband suppression. A capacitively loaded TL resonator is adopted in the design of packaged CMOS TL-based active BPF to control the spurious responses to achieve wide upper stopband suppression. The monolithic CMOS TL-based active BPF is packaged using the standard COB package and, from the equivalent circuit in Fig. 4, increasing the number of ground bondwires allows the minimized ground parasitic inductance to reduce the impact on the stopband suppression. Moreover, exactly how varying the length per bondwire affects the upper stopband suppression is analyzed. The measured S-parameters, while agreeing with the simulated ones, confirm that packaged CMOS TL-based active BPF can possess high stopband suppressions of 44.57 dB at $2f_0$ and 52.78 dB at $3f_0$. Moreover, the wide upper stopband is extended from $1.09f_0$ to $10.05f_0$, for the suppression level of 35 dB. Furthermore, how the temperature variation influences the S-parameters of the packaged CMOS TL-based active BPF is discussed, in which the central frequency shifts from 1.587 to 1.47 GHz with a shift rate of -0.9 MHz/°C from -40°C to $+80$°C.

ACKNOWLEDGMENT

The authors would like to thank the National Science Council of the Republic of China, Taiwan, for financially supporting this research under Contract No. NSC 100-2221-E-002-222-MY2. Ted Knoy is appreciated for his editorial assistance.

REFERENCES

1. Hsiao, C.-Y. and Y.-C. Chiang, "A miniaturized open-loop resonator filter constructed with floating plate overlays," *Progress In Electromagnetics Research C*, Vol. 14, 131–145, 2010.

2. Dai, G.-L. and M.-Y. Xia, "Novel miniaturized bandpass filters using spiral-shaped resonators and window feed structures," *Progress In Electromagnetics Research*, Vol. 100, 235–243, 2010.
3. Chien, H.-Y., T.-M. Shen, T.-Y. Huang, W.-H. Wang, and R.-B. Wu, "Miniaturized bandpass filter with double-folded substrate integrated waveguide resonators in LTCC," *IEEE Trans. Microw. Theory Tech.*, Vol. 57, No. 7, 1774–1782, Jul. 2009.
4. Lee, Y. C. and T. W. Kim, "A low-loss patch LTCC BPF for 60 GHz system-on-package (SoP) applications," *Progress In Electromagnetics Research Letters*, Vol. 12, 183–189, 2009.
5. Kuo, J.-T., S.-C. Tang, and S.-H. Lin, "Quasi-elliptic function bandpass filter with upper stopband extension and high rejection level using cross-coupled stepped-impedance resonators," *Progress In Electromagnetics Research*, Vol. 114, 395–405, 2011.
6. Deng, H.-W., Y.-J. Zhao, X.-S. Zhang, L. Zhang, and S.-P. Gao, "Compact quintuple-mode UWB bandpass filter with good out-of-band rejection," *Progress In Electromagnetics Research Letters*, Vol. 14, 111–117, 2010.
7. Wang, S. and R.-X. Wang, "A tunable bandpass filter using Q-enhanced and semi-passive inductors at S-band in 0.18-μm CMOS," *Progress In Electromagnetics Research B*, Vol. 28, 55–73, 2011.
8. Kulyk, J. and J. Haslett, "A monolithic CMOS 2368 ±30 MHz transformer based Q-enhanced series-C coupled resonator bandpass filter," *IEEE J. Solid-State Circuits*, Vol. 41, No. 2, 362–374, Feb. 2006.
9. Tzuang, C.-K. C., H.-H. Wu, H.-S. Wu, and J. Chen, "CMOS active bandpass filter using compacted synthetic quasi-TEM lines at C-band," *IEEE Trans. Microw. Theory Tech.*, Vol. 54, No. 12, 4548–4555, Dec. 2006.
10. Soorapanth, T. and S. S. Wong, "A 0-dB IL 2140 ± 30 MHz bandpass filter utilizing Q-enhanced spiral inductors in standard CMOS," *IEEE J. Solid-state Circuits*, Vol. 37, No. 5, 579–586, May 2002.
11. Georgescu, B., I. G. Finvers, and F. Ghannouchi, "2 GHz Q-enhanced active filter with low passband distortion and high dynamic range," *IEEE J. Solid-State Circuits*, Vol. 41, No. 9, 2029–2039, Sep. 2006.
12. Aparin, V. and P. Katzin, "Active GaAs MMIC band-pass filters with automatic frequency tuning and insertion loss control," *IEEE J. Solid-State Circuits*, Vol. 30, No. 10, 1068–1073, Oct. 1995.

13. Lee, M.-L., H.-S. Wu, and C.-K. C. Tzuang, "1.58 GHz third-order CMOS active bandpass filter with improved passband flatness," *IEEE Trans. Microw. Theory Tech.*, Vol. 59, No. 9, 2275–2284, Sept. 2011.
14. Wong, B. P., A. Mittal, Y. Cao, and G. Starr, *Nano CMOS Circuit and Physical Design*, 172–219, John Wiley & Sons, Inc., New York, 2005.
15. Matthaei, G. L., L. Young, and E. M. T. Jones, *Microwave Filters, Impedance-Matching Networks, and Coupling Structures*, 427–440, Artech House, Norwood, MA, 1980.
16. Yeung, L. K., K.-L. Wu, and Y. E. Wang, "Low-temperature cofired ceramic LC filters for RF applications," *IEEE Microw. Mag.*, Vol. 9, No. 5, 118–128, Oct. 2008.
17. Irwin, J. D. and C.-H. Wu, *Basic Engineering Circuit Analysis*, 6th edition, 729, John Wiley & Sons, Inc., New York, 1999.